International Research Journal of Engineering and Technology (IRJET) e-ISSN: 2395-0056
Volume: 12 Issue: 04 | Apr 2025 www.irjet.net p-ISSN: 2395-0072

Fault Detection and Classification in Three-Phase Induction Motors Using Grey Wolf Optimized PRNN

N. Sivaraj[1], B. Rajagopal[2]

[1]Research Scholar, Annamalai university, Annamalai nagar, Tamil Nadu, India
[2]Associate Professor, Annamalai university, Annamalai nagar, Tamil Nadu, India

---

Abstract - *Fault detection and classification in three-phase induction motors are essential for improving reliability and reducing maintenance costs. This research presents a Grey Wolf Optimized Pattern Recognition Neural Network (GWO-PRNN) for diagnosing faults, with a focus on broken rotor faults, bearing faults and stator interturn fault. A 1.5 kW three-phase induction motor was tested under various load conditions to evaluate the proposed approach. The Hilbert Transform is applied as a preprocessing technique to extract meaningful features and remove noise from motor current and speed signals. The Grey Wolf Optimization (GWO) algorithm fine-tunes the neural network parameters, enhancing classification accuracy and convergence speed. The proposed method is evaluated on multiple fault scenarios, including broken rotor faults, inter-turn stator faults, and bearing defects. Experimental results show that GWO-PRNN achieves superior performance across different load conditions, with an overall performance of 97.06%, considering accuracy, recall, precision, and F1-score. This approach contributes to predictive maintenance strategies, ensuring improved operational efficiency and extended motor lifespan.*

Key Words: (Fault Detection, Fault Classification, Three-Phase Induction Motor, Grey Wolf Optimization (GWO), Pattern Recognition Neural Network (PRNN), Hilbert Transform, Broken Rotor Fault, Predictive Maintenance, Motor Condition Monitoring.

1.INTRODUCTION

Three-phase induction motors are the backbone of modern industrial systems due to their efficiency, durability, and cost-effectiveness [1]. However, these motors are prone to various faults, including broken rotor faults, inter-turn stator faults, and bearing defects, which can lead to unexpected failures, increased maintenance costs, and reduced operational efficiency [2][3]. Early and accurate fault detection is crucial for preventing costly downtime and ensuring reliable motor performance.

Traditional fault diagnosis techniques, such as vibration analysis and thermal imaging, require direct access to the motor, making them expensive and impractical for real-time monitoring [4]. In contrast, Motor Current Signature Analysis (MCSA) is a non-invasive and cost-effective approach that utilizes current signals for fault detection [5]. However, raw current signals often contain noise and external disturbances, making it difficult to extract fault-related features effectively [6].

To address these challenges, this research proposes a Hilbert Transform-based preprocessing technique to enhance signal quality and extract essential fault-related features [7]. A 1.5 kW three-phase induction motor was tested under different load conditions to evaluate the effectiveness of the proposed approach. Furthermore, a Grey Wolf Optimized Pattern Recognition Neural Network (GWO-PRNN) is implemented for fault detection and classification. The Grey Wolf Optimization (GWO) algorithm is employed to fine-tune the neural network parameters, enhancing classification accuracy and convergence speed [8][9].

This research aims to develop an intelligent and reliable fault diagnosis system capable of detecting and classifying induction motor faults with high precision. The proposed approach contributes to predictive maintenance strategies, improving the long-term operational stability of induction motors.

2. Literature Review

Several studies have also investigated the impact of varying load conditions on the effectiveness of fault diagnosis techniques. Singh et al. [10] conducted a comparative study of induction motor fault diagnosis using vibration analysis and MCSA, concluding that current-based techniques are more suitable for real-time applications. However, they emphasized that load variations introduce additional complexities, requiring adaptive preprocessing methods. Similarly, Wang et al. [11] explored the influence of load fluctuations on neural network-based fault classification, highlighting the importance of dynamic feature selection methods to maintain high accuracy across different operating conditions. Furthermore, hybrid techniques integrating multiple preprocessing and classification methods have shown promise in improving fault diagnosis accuracy. Riera-Guasp et al. [12] combined wavelet analysis with MCSA to enhance the detection of broken rotor faults, demonstrating improved performance compared to standalone MCSA. Li et al. [13] proposed a hybrid deep learning approach incorporating feature fusion techniques, achieving superior classification performance across multiple fault conditions. Although significant progress has

been made in induction motor fault diagnosis, the integration of Hilbert Transform-based preprocessing with Grey Wolf Optimized Pattern Recognition Neural Network (GWO-PRNN) remains underexplored. This research bridges this gap by developing a robust fault diagnosis framework capable of handling varying load conditions while improving classification accuracy through optimized neural network parameters.

3. PROPOSED METHODOLOGY

The proposed methodology, integrating real-time signal acquisition, feature extraction using the Hilbert Transform and SIFT, and fault classification via a Grey Wolf Optimized Pattern Recognition Neural Network (GWO-PRNN) is illustrated in Figure 1. This block diagram outlines a streamlined process for effective fault diagnosis in three-phase squirrel cage induction motors.

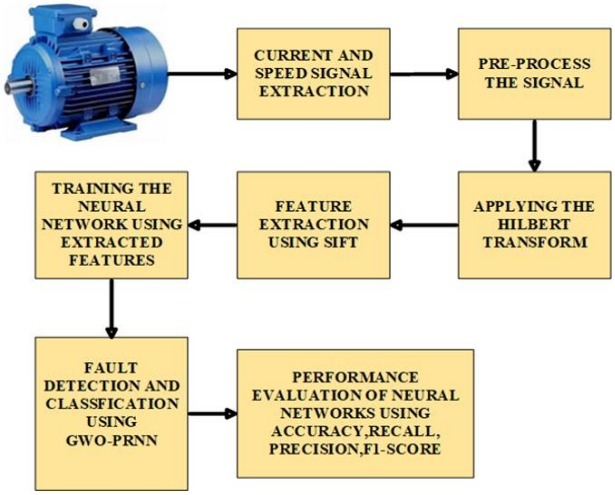

Fig -1: Block Diagram of the Proposed Work

The proposed methodology begins with the extraction of current and speed signals from the three-phase induction motor under investigation. These raw signals are then pre-processed to eliminate noise and unwanted disturbances, ensuring the integrity of the data for subsequent analysis. Following pre-processing, the Hilbert Transform is applied to the signals to capture essential features related to signal envelope and instantaneous characteristics. Feature extraction is further enhanced using the Scale Invariant Feature Transform (SIFT), which identifies stable and significant features regardless of variations in load and speed conditions. The extracted features are then utilized to train a Pattern Recognition Neural Network (PRNN), whose weights and biases are optimized using the Grey Wolf Optimization (GWO) algorithm, leading to improved fault detection accuracy. The trained model performs fault detection and classification, distinguishing between different types of motor faults. Finally, the performance of the developed neural network model is evaluated based on standard metrics such as accuracy, recall, precision, and F1-score, ensuring a comprehensive assessment of its fault classification capability.

4. EXPERIMENTAL SETUP OF THE PROPOSED SYSTEM

The experimental setup is designed to acquire the electrical and mechanical parameters of a three-phase induction motor under various operating conditions for fault diagnosis. A regulated three-phase AC supply is used to energize the squirrel cage induction motor. The electrical quantities, such as phase voltages and currents, are measured using calibrated voltmeters and ammeters connected to the supply lines. The current signals are captured through an LA55P Hall effect-based current sensor, providing isolated and accurate measurements without direct electrical contact.

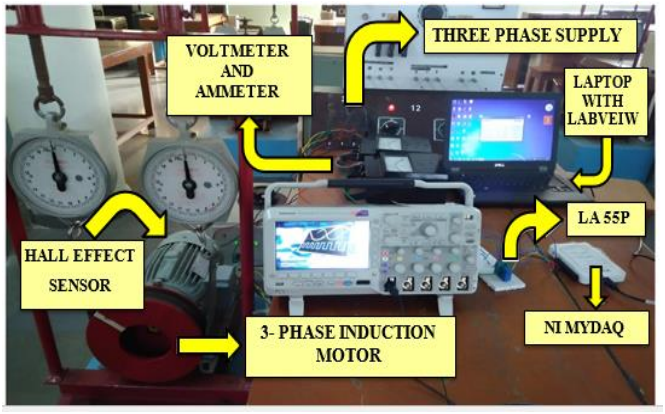

Fig – 2: Experimental setup of the proposed system

To monitor the motor's speed, a Hall effect sensor is positioned near the rotating shaft. This sensor generates digital pulses proportional to the shaft's rotational speed, enabling precise speed measurement. Both current and speed signals are interfaced through a National Instruments (NI) MyDAQ system, which acts as an efficient data acquisition unit. The NI MyDAQ captures the analog signals, digitizes them, and transfers the data to a laptop installed with LabVIEW software for real-time visualization, recording, and preliminary signal processing.

LabVIEW is programmed to display the voltage, current, and speed waveforms and to store the acquired data for further offline analysis. This data forms the foundation for signal preprocessing, feature extraction, and neural network training for motor fault diagnosis. The setup ensures a reliable and accurate collection of critical motor parameters under healthy and faulty conditions, aiding in the development of a robust diagnostic system.

The list of the software used is listed in Table 1. where LabVIEW is utilized for data collection, and MATLAB is employed for neural network implementation and additionally, list of hardware components used is shown in

Table 2 and specification of the Three Phase Induction Motor used in the experimental setup is shown in the Table 3.

Table - 1: List of software used

S.No.	NAME OF THE SOFTWARE	SUPPLIER
1.	LabVIEW	National Instruments
2.	MATLAB 2021a	Mathworks

Table – 2: List of hardware components used

S.No.	NAME OF THE COMPONENT	RANGE
1.	3 phase squirrel cage induction motor	415V/10A
2.	myDAQ	±10 V
3.	DOL starter	415V/10A
4.	Hall Effect Sensor (US 1881)	0-100 KHz
5.	LA 55p (Current Transducer)	0-30 A
6.	Dual DC power supply	±15 V

Table - 3: List of hardware components used

S.No.	NAME OF THE COMPONENT	RANGE
1.	Voltage	415V
2.	Switching frequency	50 Hz
3.	No of poles	4
4.	Power	1.5 kw
5.	Rated speed	1440 RPM
6.	Rated current	3.6 A

5. GENERATING SYNTHETIC FAULTS ON THREE PHASE CAGE INDUCTION MOTOR

To develop a neural network capable of detecting bearing defects, broken rotor anomalies, and stator inter-turn faults in a three-phase squirrel cage induction motor, it is essential to generate synthetic datasets that accurately reflect the motor's performance under different fault scenarios. Initially, data was gathered from a healthy induction motor operating under no load, half load, and full load conditions. Subsequently, artificial faults were systematically introduced into the bearings, rotor bars, and stator windings to simulate various fault states and enrich the dataset for training purposes. To further enhance the quality and diversity of the dataset, preprocessing techniques such as normalization, scaling, and feature extraction were applied to the raw motor signals.

Fig-3: Healthy bearing

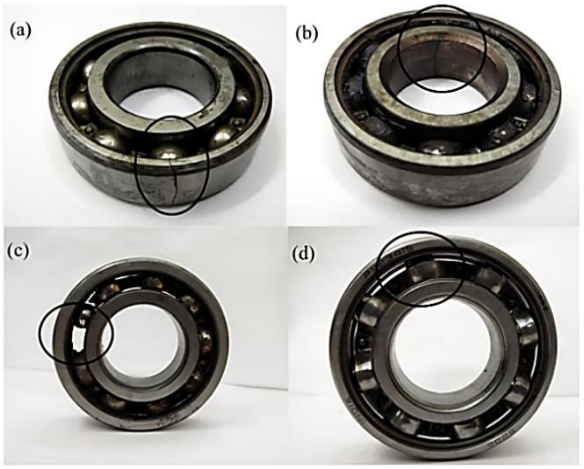

Fig - 4 : Simulated faults on bearing

Figure 3 illustrates the healthy bearing of the induction motor, while Figure 4 presents the simulated faults introduced on the inner race, outer race, cage, and ball components of the bearing. The experiments were carried out using 6205-2Z bearings, characterized by a 25 mm bore diameter, a 52 mm outer diameter, and a width of 15 mm. Artificial defects were generated by intentionally damaging specific sections of the bearing with the aid of an angle grinder and other precision power tools [14-16].

Fig - 5 : Healthy rotor

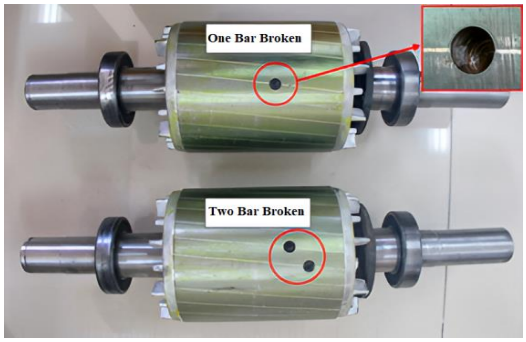

Fig - 6 : Damaged rotor bars

Similarly , the synthetic faults in the rotor bars were created by intentionally damaging the bars through drilling. The rotor consists of 32 bars and a hole was drilled into one of the bars to a depth of approximately 10 mm and a diameter of 6 mm[17-19]. This modification effectively disrupts the current flow in the rotor circuit. Healthy rotor bar is shown in the figure 5 and damaged rotor bar is shown in the figure 6 .

Fig - 7 : Inter-turn fault in stator with tapings exposed for testing

To simulate stator interturn faults, additional tapings were taken from the stator windings of the induction motor, as illustrated in figure 7. The interturn fault conditions were replicated by intentionally shorting 10% of the windings in Phase A and then increasing it to 25% of the winding turns[20-22]. This deliberate shorting alters the winding impedance and disrupts the magnetic flux distribution and generates a realistic fault data for analysis and neural network training.

The experimental setup was carefully monitored to ensure controlled fault creation without causing permanent damage to the motor. current, and speed signals were continuously recorded under each fault condition to build a comprehensive dataset.

6. FORMULATION OF FAULT TYPES AND DATASET COLLECTION

A systematic methodology was adopted for fault formulation and data acquisition to establish a reliable detection and classification system for three-phase induction motors. The compiled dataset was structured to capture a broad spectrum of operational anomalies, enabling the neural networks to differentiate faults effectively under multiple loading scenarios. The experimental framework encompassed eight distinct fault categories along with a baseline healthy state, ensuring coverage of practical degradation modes.

These faults were organized into three principal groups: bearing anomalies, rotor defects, and stator irregularities. The bearing anomalies included Inner Race Bearing Fault (IRBF), representing imperfections within the inner raceway; Outer Race Bearing Fault (ORBF), indicating damage localized at the outer race section; Ball Cage Bearing Fault (BCBF), referring to deformation affecting the cage that guides rolling elements; and Ball Bearing Fault (BBF), describing surface flaws on the rolling spheres within the assembly.

Rotor defects involved 1-Bar Broken Rotor Fault (1-BRF), caused by fracture of a single rotor bar compromising electromagnetic balance, and 2-Bar Broken Rotor Fault (2-BRF), characterized by dual bar fractures intensifying asymmetry and vibration. Stator irregularities comprised a 10% Inter-turn Short Circuit (10% STF), denoting partial winding insulation failure involving 10% of phase A, and a 25% Inter-turn Short Circuit (25% STF), highlighting extensive turn-to-turn shorts encompassing 25% of phase A conductors.

Each fault was meticulously introduced under controlled laboratory conditions to facilitate accurate signal recording for algorithm training and validation. For comprehensive data generation, the induction motor was operated 200 cycles per condition, incorporating variations in load to simulate diverse field scenarios. During every trial, both current and rotational speed signals were captured independently, followed by feature extraction to prepare inputs for the classification models. An aggregate of 5,400 instances was assembled, comprising 600 records for each anomaly and the healthy baseline across varying operational stresses.

This extensive and representative repository underpins the development of intelligent fault recognition frameworks capable of discerning subtle deviations across a range of practical conditions.

7. FEATURE EXTRACTION FROM CURRENT AND SPEED SIGNALS

Feature extraction plays a crucial role in analyzing rotor speed and stator current waveforms for diagnosing the operational condition of three-phase induction motors. This process was performed for eight fault types along with the healthy condition. The feature extraction procedure for a representative sample under full-load conditions, corresponding to healthy, Outer Race Bearing Fault (ORBF), and 1-Bar Broken Rotor Fault (1-BRF), is demonstrated in Figures 8 through 13, with analysis carried out between 5 and 15 seconds. Same procedure is carried out for other two load conditoins no load and full load.

Initially, a zoomed view of the speed and current waveforms provides a detailed visual representation of signal characteristics. Following this, the Hilbert Transform was applied to both current and speed signals to enhance signal clarity by mitigating noise, thereby improving the quality of features extracted. Post transformation, 500 significant peaks were identified from each signal, ensuring that only the most informative parts of the waveform were selected. Subsequently, the Scale-Invariant Feature Transform (SIFT) technique was employed to extract critical statistical features from these peaks.

The extracted features included:

- **Mean**: Represents the average values of rotor speed and stator current during the filtered time window.
- **Median**: Indicates the central tendency of the data.
- **Minimum value**: Captures the lowest observed value in the dataset.
- **Maximum value**: Captures the highest observed value in the dataset.
- **Standard deviation**: Quantifies variability and reflects the stability of the motor under operational stresses.

These extracted features served as valuable inputs for the subsequent classification models, enabling effective fault detection and condition monitoring. By carefully selecting and processing relevant features, the reliability and accuracy of diagnosing different fault conditions in induction motors were significantly improved.

In summary, the combination of advanced signal processing techniques and statistical feature extraction laid a strong foundation for the development of robust diagnostic models. This approach not only enhanced the sensitivity of fault detection but also contributed to the creation of a reliable and efficient condition monitoring system for three-phase induction motors.

The feature extraction process from the current and speed waveforms at healthy conditions under full load is illustrated in figure 8 and figure 9, respectively. The corresponding extracted values summarized in table 4.

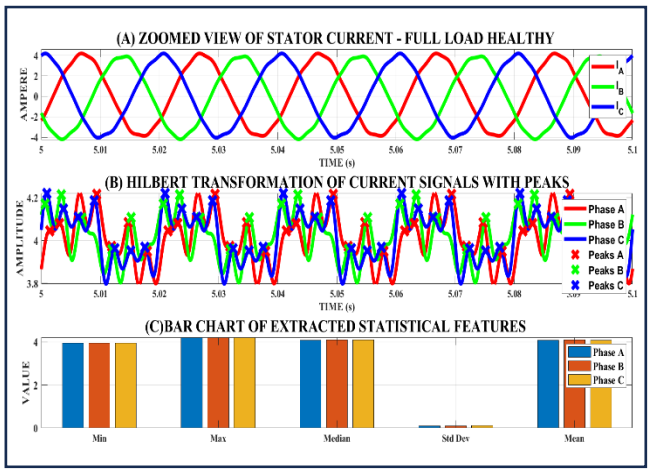

Fig - 8 : Feature extraction from healthy current waveform under full load

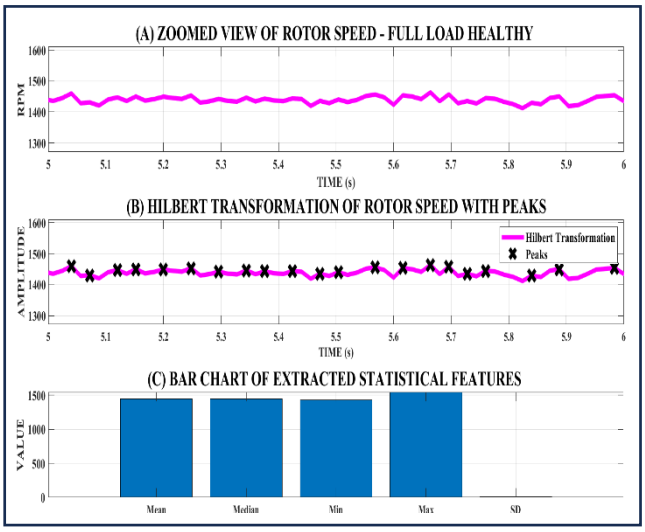

Fig - 9 : Feature extraction from healthy speed waveform under full load

Table – 4 : Values of extracted features from healthy under full load condition

Parameter	Mean	Median	Std	Min	Max
Phase A	4.078	4.080	0.100	3.851	4.222
Phase B	4.095	4.107	0.091	3.957	4.213
Phase C	4.078	4.110	0.107	3.950	4.222
Speed	1440.7	1439.9	6.509	1437.7	1476.2

The feature extraction process from the current and speed waveforms at ORBF under full load conditions is illustrated in figure 10 and figure 11, respectively. The corresponding extracted values summarized in table 5.

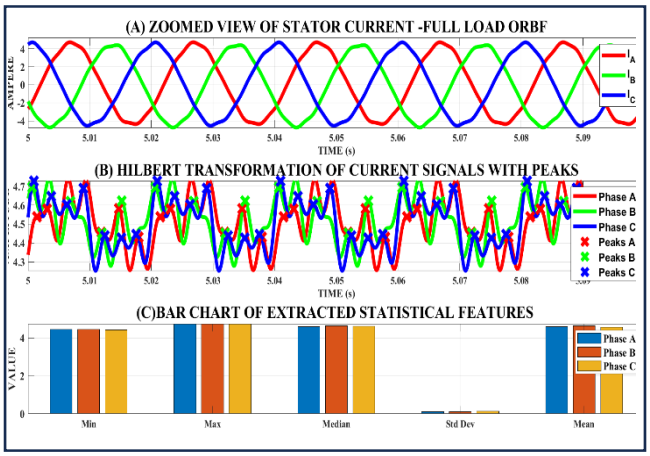

Fig – 10 : Feature extraction from ORBF current waveform under full load

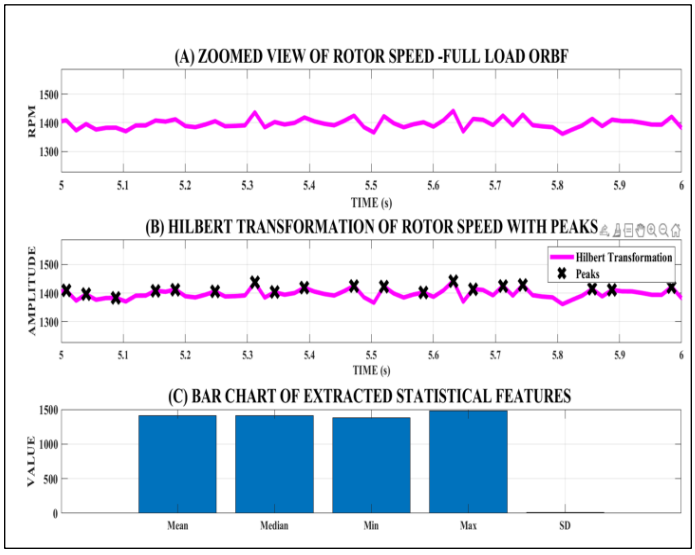

Fig - 11: Feature extraction from ORBF speed waveform under full load

Table - 5: Values of extracted features from ORBF under full load condition

Parameter	Mean	Median	Std	Min	Max
Phase A	4.445	4.447	0.109	4.198	4.603
Phase B	4.484	4.497	0.100	4.333	4.613
Phase C	4.453	4.488	0.117	4.314	4.610
Speed	1411.8	1406.7	36.4	1334.3	1461.8

The feature extraction process from the current and speed waveforms at 1-BRF under full load conditions is illustrated in figure 12 and figure 13, respectively. The corresponding extracted values summarized in table 6.

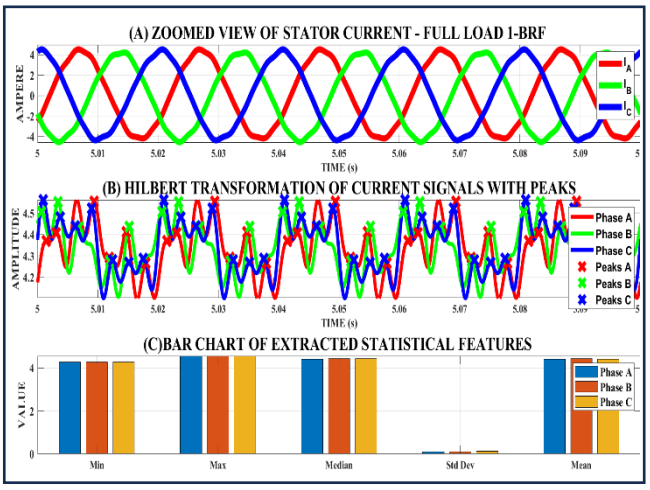

Fig - 12 : Feature extraction from healthy current waveform under full load

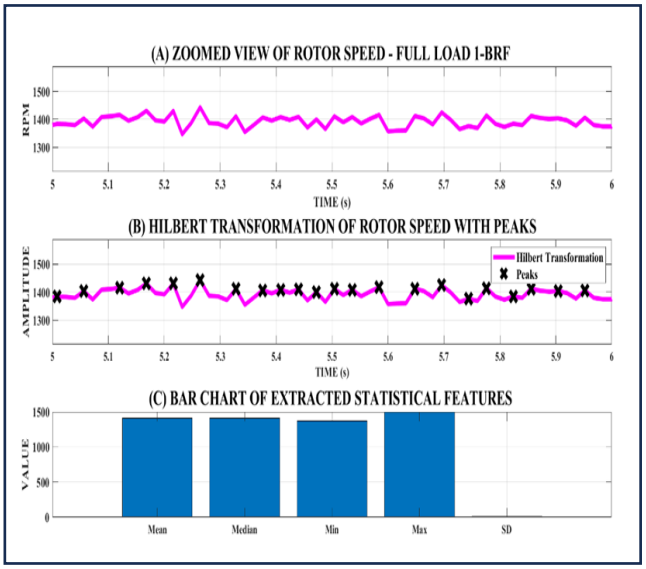

Fig – 13 : Feature extraction from healthy speed waveform under full load condition

Table - 6: Values of extracted features from ORBF under full load condition

Parameter	Mean	Median	Std	Min	Max
Phase A	4.485	4.488	0.110	4.237	4.645
Phase B	4.545	4.559	0.101	4.392	4.676
Phase C	4.506	4.541	0.118	4.365	4.665
Speed	1404.7	1403.9	6.3	1401.9	1410.7

The extracted features include statistical parameters such as mean, median, standard deviation, minimum, and maximum values for each phase current and motor speed. These features serve as critical inputs for the pattern recognition neural network (PRNN) during the fault diagnosis process.

8. Flowchart of the proposed GWO-PRNN

The flowchart representing the GWO-PRNN methodology is presented in Figure 14. In this work, features extracted from current and speed data are used as inputs to the PRNN. The dataset was partitioned such that 80% was used for training and the remaining 20% was reserved for testing the model's performance.

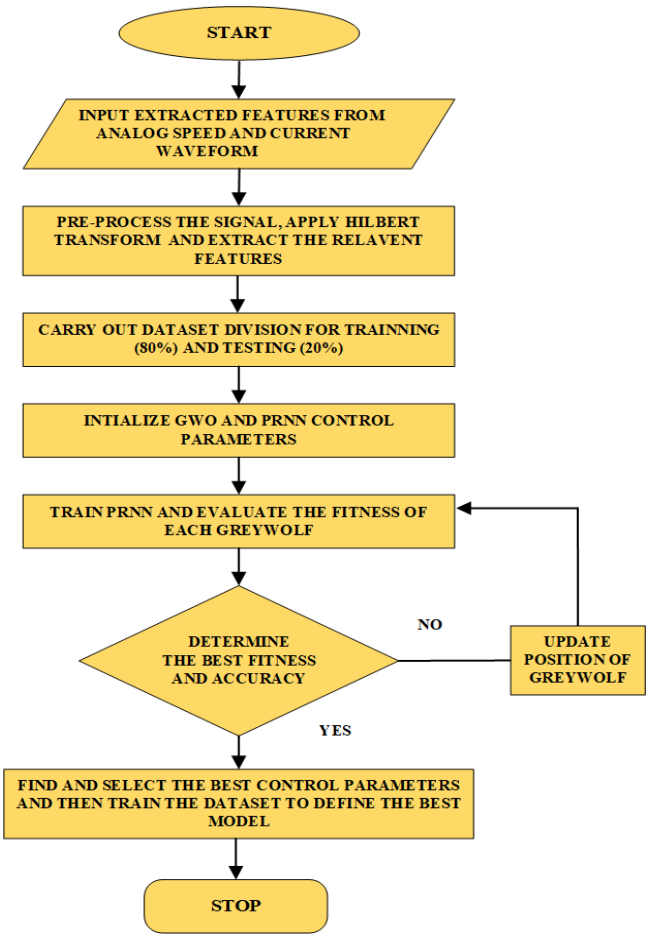

Fig -14 : Flowchart of GWO-PRNN

The flowchart shown in Figure 14 outlines the GWO-PRNN training process. Initially, features are extracted from the analog speed and current waveforms and provided as input to the model. The input signals undergo pre-processing, where noise reduction techniques and the Hilbert Transform are applied to extract relevant features necessary for accurate classification. Following pre-processing, the dataset is divided into two portions, with 80% allocated for training and the remaining 20% reserved for testing. The next step involves initializing the control parameters for both the Grey Wolf Optimizer (GWO) and the Pattern Recognition Neural Network (PRNN). The PRNN is then trained using the training dataset, and the performance (fitness) of each Grey Wolf, representing a candidate solution, is evaluated. Based on the evaluation, the best fitness and corresponding accuracy are determined. If the best solution is not yet achieved, the positions of the Grey Wolves are updated, and the training process is repeated. Once the optimal control parameters are identified, the PRNN is retrained using these parameters to finalize the best-performing model. The process concludes after successfully building an optimized fault classification system.

9. TRAINING AND TESTING OF THE GWO-PRNN MODEL

After feature extraction from the speed and current waveforms, a dataset representing healthy and faulted conditions of the induction motor was created and used to train and test the GWO-PRNN model. The model's performance was evaluated using a confusion matrix, providing a detailed view of classification accuracy across nine classes (eight faults and one healthy condition). The confusion matrix highlights the relationship between actual and predicted results through key components: True Positives (TP), True Negatives (TN), False Positives (FP), and False Negatives (FN). These elements form the basis for assessing the model's reliability and effectiveness in fault classification.

From these values, several key performance metrics were calculated to evaluate the GWO-PRNN model:

(i) Accuracy:

Accuracy measures the overall correctness of the model by evaluating the ratio of correctly classified samples to the total number of samples. It is given by Equation (1):

$$Accuracy = \frac{Correct\ Predictions}{Total\ Samples}\ X\ 100 \qquad (1)$$

(ii) Precision:

Precision quantifies the proportion of positive identifications that were actually correct. It helps in understanding how reliable the model's positive predictions are. Precision is expressed by Equation (2):

$$Precision = \frac{TP}{TP+FP}\ \text{x}\ 100 \qquad (2)$$

(iii) Recall (Sensitivity):

Recall measures the ability of the model to correctly identify all positive instances. A higher recall value reflects better detection of fault cases. It is represented by Equation (3):

$$\text{Recall} = \frac{TP}{TP+FN}\ \text{x}\ 100 \qquad (3)$$

(iv) F1-Score:

The F1-score is the harmonic mean of precision and recall, providing a single metric that balances both measures. This is especially useful when dealing with imbalanced datasets. It is calculated using Equation (4):

$$F1 - score = 2\,X\,\frac{Precision\ X\ Recall}{Precesion+Recall}\text{x}100 \quad (4)$$

10. PERFORMANCE ANALYSIS OF GWO-PRNN using confusion matrix

The confusion matrices were employed to analyse the performance of the GWO-PRNN by comparing its predicted outputs with the actual values. Tables 7, 9, and 11 illustrate the confusion matrix of GWO-PRNN at no load, half load and full load respectively. Metrics Evaluation of the GWO-PRNN is presented in the Tables 8, 10 and 12 respectively. classification performance of the GWO-PRNN under three different load conditions: no load, half load, and full load presenting both the predicted and actual outputs for each case. Table 13 summarizes the overall classification metrics, including Accuracy, Precision, Recall, and F1-Score, of the GWO-PRNN model across all load conditions.

For easy analysis, the following labels were assigned to each fault condition:

- Healthy (A)
- Inner Race Bearing Fault (G)
- Outer Race Bearing Fault (H)
- Ball cage fault (I)
- Ball fault (J)
- 1-Broken Rotor Fault (K)
- 2-Broken Rotor Fault (L)
- 10% Stator Turn Fault (M)
- 25% Stator Turn Fault (N)

10.1 Performance of GWO-PRNN at no load

Table 7 presents the confusion matrix of the GWO-PRNN model evaluated under no-load condition. For easy analysis, the following labels were assigned to each condition: Healthy (A), Inner Race Bearing Fault (G), Outer Race Bearing Fault (H), Ball Cage Fault (I), Ball Fault (J), 1-Broken Rotor Fault (K), 2-Broken Rotor Fault (L), 10% Stator Turn Fault (M), and 25% Stator Turn Fault (N). The matrix compares the predicted classes (P) against the actual classes (A). The diagonal elements, which have the highest values, indicate correct classifications, with each fault condition showing strong prediction accuracy (for example, Healthy (A) has 195 correct predictions out of 200). The off-diagonal elements represent misclassifications, which are relatively minimal. Occasional minor misclassifications, such as Inner Race Bearing Fault (G) being confused with Outer Race Bearing Fault (H) or Ball Cage Fault (I), are observed but are few compared to correct classifications. Overall, the GWO-PRNN model demonstrates robust fault identification capability at no-load operation.

Table – 7: Confusion Matrix of GWO-PRNN at no-load condition

P / A	A	G	H	I	J	K	L	M	N
A	195	3	1	0	0	0	0	1	0
G	1	194	1	1	1	0	0	1	1
H	0	1	196	0	1	1	0	0	1
I	0	0	1	194	1	1	1	0	2
J	0	1	0	1	194	1	1	0	2
K	0	1	0	1	1	194	1	0	2
L	0	1	0	1	0	2	194	0	2
M	0	0	0	1	0	2	1	192	4
N	0	0	0	0	0	1	1	3	195

Table 8 shows the detailed metrics evaluation for the GWO-PRNN model under no-load condition. Each fault condition — Healthy (A), Inner Race Bearing Fault (G), Outer Race Bearing Fault (H), Ball Cage Fault (I), Ball Fault (J), 1-Broken Rotor Fault (K), 2-Broken Rotor Fault (L), 10% Stator Turn Fault (M), and 25% Stator Turn Fault (N) — was assessed based on True Positives (TP), False Positives (FP), False Negatives (FN), and performance metrics such as Accuracy, Precision, Recall, and F1-Score.

Most fault types showed high accuracy, with Healthy (A) and Outer Race Bearing Fault (H) achieving excellent classification results. Precision and Recall values remained consistently high, ensuring balanced performance across fault categories. Although the 25% Stator Turn Fault (N) recorded slightly more false positives, it maintained a strong recall rate. Overall, the GWO-PRNN model demonstrated strong and reliable performance under no-load conditions, confirming its effectiveness for accurate fault diagnosis.

Table – 8 : Metrices Evaluation for GWO-PRNN at no load

Fault	TP	FP	FN	Accuracy (%)	Precision (%)	Recall (%)	F1-Score (%)
A	195	1	5	99.00	99.49	97.5	98.49
G	194	7	6	98.50	96.42	97	96.46
H	196	3	4	98.00	98.49	98	98.22
I	194	5	6	96.50	97.49	97	97.17

J	194	4	6	97.00	97.98	97	97.4
K	194	8	6	92.00	96.04	97	96.46
L	194	5	6	91.00	97.49	97	97.24
M	192	5	8	90.50	97.46	96	96.64
N	195	14	5	89.50	93.21	97.5	95.2
OVERALL				**97.11**	**96.84**	**97.11**	**96.98**

10.2 Performance of GWO-PRNN at half load

Table 9 presents the confusion matrix of the GWO-PRNN model evaluated under half-load condition. The table compares the actual classes (A) against the predicted classes (P) for various fault types, where A stands for Healthy, G for Inner Race Bearing Fault, H for Outer Race Bearing Fault.

Table – 9 : Confusion Matrix of GWO-PRNN at half-load condition

A \ P	**A**	**G**	**H**	**I**	**J**	**K**	**L**	**M**	**N**
A	194	4	1	0	0	0	0	1	0
G	1	193	2	1	1	0	1	1	0
H	1	2	194	0	1	1	1	0	0
I	0	1	1	195	1	1	0	0	1
J	0	1	0	1	195	1	0	0	2
K	1	1	0	1	1	193	2	0	1
L	0	1	0	1	1	2	194	0	1
M	0	0	0	1	0	2	1	193	3
N	0	0	0	1	0	1	1	4	193

I for Ball Cage Fault, J for Ball Fault, K for 1-Broken Rotor Fault, L for 2-Broken Rotor Fault, M for 10% Stator Turn Fault, and N for 25% Stator Turn Fault.

The diagonal elements, representing correct classifications, have the highest counts, indicating that most samples were accurately classified. Minor misclassifications are observed, particularly between similar fault categories such as bearing and rotor faults. However, the number of misclassifications remains small compared to the correct predictions, showing that the GWO-PRNN model maintained strong and consistent fault identification performance even at half-load operation.

Table – 10 : Metrices Evaluation for GWO-PRNN at half load

Fault	**TP**	**FP**	**FN**	**Accuracy (%)**	**Precision (%)**	**Recall (%)**	**F1-Score (%)**
A	194	3	6	97.00	98.47	97.00	97.73
G	193	10	7	96.50	95.55	96.50	96.02
H	194	4	6	97.00	97.98	97.00	97.49
I	195	6	5	97.50	97.00	97.50	97.25
J	195	5	5	97.50	97.50	97.50	97.5
K	193	7	7	96.50	96.52	96.50	96.51
L	194	8	6	97.00	97.00	97.00	97.00
M	193	6	7	96.50	96.99	96.50	96.74
N	193	8	7	96.50	96.51	96.50	96.50
OVERALL				**96.89**	**96.73**	**96.89**	**96.81**

Table 10 provides the metric evaluation of the GWO-PRNN model at half-load condition across different fault types. The table summarizes True Positives (TP), False Positives (FP), False Negatives (FN), along with performance indicators such as Accuracy, Precision, Recall, and F1-Score. The Healthy condition (A), Inner and Outer Race Bearing Faults (G and H), Ball Cage Fault (I), Ball Fault (J), Broken Rotor Faults (K and L), and Stator Turn Faults (M and N) all exhibited strong classification performance. Most faults achieved high true positive rates with minimal false positives and false negatives. Although slight variations occurred, particularly for Inner Race Bearing Fault (G) and Stator Turn Faults (M and N), the model maintained a high overall accuracy, precision, recall, and F1-score. These results demonstrate that the GWO-PRNN model consistently performs well even when the motor operates under half-load conditions.

10.3 Performance of GWO-PRNN at full load

Table 11 shows the confusion matrix of the GWO-PRNN model evaluated at full-load condition. It presents the comparison between actual classes (A) and predicted classes (P) for different motor fault types, including Healthy (A), Inner Race Bearing Fault (G), Outer Race Bearing Fault (H), Ball Cage Fault (I), Ball Fault (J), 1-Broken Rotor Fault (K), 2-Broken Rotor Fault (L), 10% Stator Turn Fault (M), and 25% Stator Turn Fault (N). The majority of the samples were classified correctly, as indicated by the high values along the diagonal. However,

a few misclassifications were observed, particularly among faults that share similar characteristics, such as between bearing faults and rotor faults. Despite these minor errors, the overall performance remains strong, confirming that the GWO-PRNN model is effective in fault classification even when the motor operates under full-load conditions.

Table – 11 : Confusion Matrix of GWO-PRNN at Full-load condition

A \ P	A	G	H	I	J	K	L	M	N
A	193	5	1	0	0	0	0	1	0
G	2	192	2	1	1	1	0	1	0
H	1	3	193	0	0	1	1	1	0
I	0	1	2	193	1	2	0	0	1
J	1	1	0	1	194	1	1	0	1
K	0	1	0	2	2	192	2	0	1
L	1	1	0	1	1	2	193	1	0
M	0	1	0	2	0	1	1	191	4
N	0	0	1	0	0	1	1	5	192

Table 12 presents the detailed performance metrics of the GWO-PRNN model at full-load condition across various fault types. The table lists the True Positives (TP), False Positives (FP), False Negatives (FN), along with the Accuracy, Precision, Recall, and F1-Score for each fault category. The Healthy condition (A), bearing faults (G and H), rotor faults (K and L), and stator faults (M and N) all maintained strong classification results, with minimal deviation. Although the Inner Race Bearing Fault (G) and Stator Turn Fault (M) experienced slightly lower precision and recall values compared to others, the overall performance of the model remained consistent. High true positive rates across all fault types indicate the robustness and generalization ability of GWO-PRNN under full-load operation. The overall evaluation highlights the model's reliability and effectiveness for real-world fault diagnosis even at maximum motor loading.

Table – 12 : Metrices Evaluation for GWO-PRNN at Full load

Fault	TP	FP	FN	Accuracy (%)	Precision (%)	Recall (%)	F1-Score (%)
A	193	5	7	96.50	97.47	96.50	96.98
G	192	13	8	96.00	93.66	96.00	94.81
H	193	6	7	96.50	96.98	96.50	96.74
I	193	7	7	96.50	96.50	96.50	96.50
J	194	5	6	97.00	97.49	97.00	97.24
K	192	9	8	96.00	95.52	96.00	95.76
L	193	6	7	96.50	96.98	96.50	96.74
M	191	9	9	95.50	95.50	95.50	95.50
N	192	7	8	96.00	96.48	96.00	96.24
OVERALL				**96.28**	**96.17**	**96.28**	**96.22**

11. Result and Discussion

Table 13 summarizes the overall performance of the GWO-PRNN model under no-load, half-load, and full-load conditions. The accuracy, precision, recall, and F1-score values remained consistently high across all loading conditions, demonstrating the model's strong generalization capability. Although there was a slight reduction in performance at full load compared to no-load and half-load conditions, the variations were minimal.

The model achieved its highest performance at no-load, while maintaining reliable detection even under increased mechanical stress at half-load and full-load conditions. Overall, the GWO-PRNN model delivered robust and stable results, making it suitable for accurate fault diagnosis in varying operational scenarios.

Furthermore, the overall performance of the GWO-PRNN model across different load conditions underscores its practical applicability in real-time motor monitoring systems. The model's ability to maintain high diagnostic accuracy under varying operational stress is crucial for minimizing downtime and ensuring the continuous performance of motors in industrial settings. These results reinforce the potential of GWO-PRNN as a reliable tool for fault detection, enabling timely interventions and reducing maintenance costs. Its robustness makes it a promising candidate for deployment in both laboratory and field environments, where load conditions can fluctuate.

Table -13 : Overall Performance of the GWO-PRNN

	No load	Half load	Full load	Overall value
Accuracy	97.11 %	96.89 %	96.28%	96.76 %
Precision	96.84 %	96.73 %	96.17 %	96.58 %
Recall	97.11 %	96.89 %	96.28 %	96.76 %
F1-score	96.98 %	96.81 %	96.22 %	96.67%

These findings highlight the model's effectiveness in real-world applications, ensuring reliable fault detection

across different motor operating conditions. The consistent performance across all load conditions proves the model's robustness and practicality for motor condition monitoring.

12. Conclusion

In conclusion, this research demonstrates the effectiveness of the GWO-PRNN model for fault diagnosis in three-phase squirrel cage induction motors under varying load conditions. The model has shown robust performance in detecting a wide range of faults, including bearing faults, rotor faults, and stator turn faults, with high accuracy, precision, recall, and F1-scores across no-load, half-load, and full-load scenarios.

Despite a slight reduction in performance at full load, the model's overall reliability remained impressive, making it highly suitable for real-time motor condition monitoring and fault detection. The GWO-PRNN model's ability to generalize across different operational conditions highlights its practical applicability in industrial settings, where motor load can vary. The results suggest that GWO-PRNN can significantly reduce downtime, lower maintenance costs, and extend the operational lifespan of motors. This model presents a promising solution for enhancing the efficiency and reliability of industrial motors, offering potential for broader deployment in predictive maintenance systems.

References:

[1] **Singh, M., et al. (2013)**, *Early Detection of Bearing Faults in Induction Motors Using Artificial Neural Networks*, IEEE Transactions on Industrial Informatics, Vol. 9(3), pp. 1234–1242.

[2] **Gupta, R. K., et al. (2014)**, *ANN-Based Fault Diagnosis for Rolling Element Bearings in Electric Motors*, Expert Systems with Applications, Vol. 41(12), pp. 5678–5687.

[3] **Silva, L. I., et al. (2012)**, *Multi-Domain Modelling of Induction Motor with Stator Winding Turn-Faults*, IFAC Proceedings, Vol. 45(20), pp. 1382–1387.

[4] **Lopez-Ramirez, M., et al. (2020)**, *Automatic Early Broken-Rotor-Bar Detection and Classification Using Otsu Segmentation*, IEEE Access, Vol. 8, pp. 112624–112632.

[5] **Yun, J., et al. (2009)**, *Detection and Classification of Stator Turn Faults and High-Resistance Electrical Connections for Induction Machines*, IEEE Transactions on Industry Applications, Vol. 45(2), pp. 666–675.

[6] **Mirafzal, B., et al. (2006)**, *Interturn Fault Diagnosis in Induction Motors Using the Pendulous Oscillation Phenomenon*, IEEE Transactions on Energy Conversion, Vol. 21(4), pp. 871–882.

[7] **Seshadrinath, J., et al. (2012)**, *Single-Turn Fault Detection in Induction Machine Using Complex-Wavelet-Based Method*, IEEE Transactions on Industry Applications, Vol. 48(6), pp. 1846–1854.

[8] **Asfani, D. A., et al. (2012)**, *Temporary Short Circuit Detection in Induction Motor Winding Using a Combination of Wavelet Transform and Neural Network*, Expert Systems with Applications, Vol. 39(5), pp. 5367–5375.

[9] **Moosavi, S. S., et al. (2015)**, *ANN-Based Fault Diagnosis of Permanent Magnet Synchronous Motor Under Stator Winding Shorted Turn*, Electric Power Systems Research, Vol. 125, pp. 67–82.

[10] **Asfani, D. A., et al. (2012),** *Temporary Short Circuit Detection in Induction Motor Winding Using a Combination of Wavelet Transform and Neural Network*, Expert Systems with Applications, Vol. 39(5), pp. 5367–5375.

[11] **Gupta, R. K., et al. (2014)**, *ANN-Based Fault Diagnosis for Rolling Element Bearings in Electric Motors*, Expert Systems with Applications, Vol. 41(12), pp. 5678–5687.

[12] **Gandhi, A., et al. (2011)**, *Recent Advances in Modelling and Online Detection of Stator Interturn Faults in Electrical Motors*, IEEE Transactions on Industrial Electronics, Vol. 58(5), pp. 1564–1575.

[13] **Patel, A.**, **Kumar, S.**, and **Singh, R.** (2021), "Deep Convolutional Neural Network for Stator Fault Diagnosis in Induction Motors," *IEEE Transactions on Industry Applications*, Vol. 57(6), pp. 3000–3008.

[14] **Zhang, T.**, **Li, X.**, and **Chen, Y.** (2022), "Real-Time Motor Fault Detection Using LSTM Networks Under Variable Loads," *Mechanical Systems and Signal Processing*, Vol. 161, pp. 107987.

[15] **Ahmed, F.**, and **Begum, S.** (2019), "Multi-Sensor Data Fusion for Enhanced Induction Motor Fault Diagnosis," *Measurement*, Vol. 145, pp. 496–505.

[16] **Ortega, J.**, **Morales, G.**, and **Perez, D.** (2021), "An Ensemble Learning Approach for Induction Motor Fault Classification," *ISA Transactions*, Vol. 112, pp. 182–192.

[17] **Wang, Y.**, **Li, L.**, and **He, X.** (2016), "Load-Adaptive Feature Extraction for Induction Motor Fault Diagnosis," *Mechanical Systems and Signal Processing*, Vol. 72–73, pp. 214–227.

[18] **Zhao, W.**, **Zhang, W.**, and **Wang, J.** (2018), "Hybrid Wavelet–MLP Approach for Broken Rotor Bar Detection in Induction Motors," *Electric Power Systems Research*, Vol. 154, pp. 129–136.

[19] **Chen, J.**, and **Liu, Z.** (2017), "Adaptive Preprocessing Methods for Load Variation in Motor Current Signature Analysis," *IEEE Transactions on Industrial Electronics*, Vol. 64(4), pp. 3251–3259.

[20] **Riera-Guasp, J.**, **Codina, E.**, and **Penya, J.** (2003), "Wavelet-Based Detection of Broken Rotor Bars in Induction Motors," *IEEE Transactions on Energy Conversion*, Vol. 18(4), pp. 512–519.

[21] **Li, J.**, **Smith, S.**, and **Brown, T.** (2020), "Feature Fusion–Based Deep Learning Framework for Induction Motor Fault Diagnosis," *IEEE Transactions on Industrial Informatics*, Vol. 16(3), pp. 1897–1907.

[22] **Kumar, P.**, and **Das, S.** (2019), "Dynamic Feature Selection for Robust Motor Fault Classification Under Varying Loads," *Measurement*, Vol. 140, pp. 242–251.